Xia, J., Chen, C., Li, P. H. & Lewis, M. J. (2004). *Géotechnique* **54**, No. 1, 17–27

Delineation of a collapse feature in a noisy environment using a multichannel surface wave technique

J. XIA*, C. CHEN†, P. H. LI‡ and M. J. LEWIS§

A collapse developed at Calvert Cliffs Nuclear Power Plant, Maryland, in early 2001. The location of the collapse was over a groundwater drainage system pipe buried at an elevation of +0·9 m (reference is to Chesapeake Bay level). The cause of the collapse was a subsurface drain pipe that collapsed because of saltwater corrosion of the corrugated metal pipe. The inflow/outflow of sea water and groundwater flow caused soil to be removed from the area where the pipe collapsed. To prevent damage to nearby structures, the collapse was quickly filled with uncompacted sand and gravel (~36 000 kg). However, the plant had an immediate need to determine whether more underground voids existed. A high-frequency multichannel surface-wave survey technique was conducted to define the zone affected by the collapse. Although the surface-wave survey at Calvert Cliffs Nuclear Power Plant was conducted at a noise level 50–100 times higher than the normal environment for a shallow seismic survey, the shear (S)-wave velocity field calculated from surface-wave data delineated a possible zone affected by the collapse. The S-wave velocity field showed chimney-shaped low-velocity anomalies that were directly related to the collapse. Based on S-wave velocity field maps, a potential zone affected by the collapse was tentatively defined.

Un effondrement s'est développé à la centrale nucléaire de Calvert Cliffs dans le Maryland au début de 2001. L'effondrement était situé au-dessus d'une canalisation de drainage d'une nappe d'eau souterraine, enterrée à une hauteur de +0,9 m (au niveau de Chesapeake Bay). La cause de cet effondrement était la défaillance de la canalisation de drainage souterraine en raison de la corrosion par l'eau salée du métal ondulé. Le va-et-vient de l'eau de mer dans la canalisation et l'écoulement de la nappe d'eau ont fait que le sol s'est écarté de l'endroit où la canalisation s'est effondrée. Pour empêcher que les structures voisines ne soient endommagées, l'effondrement a été rapidement rempli avec du sable et du gravier non compactés (~36 000 kg). Cependant, l'usine devait absolument déterminer si d'autres vides souterrains existaient. Une technique d'étude surface-onde à multicanaux à haute fréquence a été menée pour définir la zone affectée par l'effondrement. Bien que l'étude surface-onde dans la centrale de Calvert Cliffs ait été conduite à un niveau de bruit de 50 à 100 fois supérieur à la normale pour une étude sismique peu profonde, le champ de vélocité d'onde de cisaillement (S) calculé d'après les données surface-onde a fait apparaître une zone qui pourrait être affectée par l'effondrement. Le champ de vélocité de l'onde S a montré des anomalies à faible vélocité en forme de cheminées, directement liées à l'effondrement. En nous basant sur les cartes de champ de vélocité de l'onde S, nous avons essayé de définir une zone potentiellement affectée par l'effondrement.

KEYWORDS: case history; environmental engineering; *in situ* testing; tunnels

INTRODUCTION

Elastic properties of near-surface materials and their effects on seismic wave propagation are of fundamental interest in groundwater, engineering, and environmental studies. Shear (S)-wave velocity is a key parameter in construction engineering. As an example, Imai & Tonouchi (1982) studied P- and S-wave velocities in an embankment, and also in alluvial, diluvial and tertiary layers, showing that S-wave velocities in such deposits correspond to the *N*-value (blow count) (Clayton, 1993; Clayton *et al.*, 1995), an index value of formation hardness in soil mechanics and foundation engineering.

Surface waves are guided and dispersive. Rayleigh waves are surface waves that travel along a 'free' surface, such as the earth–air interface. Rayleigh waves are the result of interfering P and S_v waves. The particle motion of Rayleigh waves moving from left to right in a homogeneous medium is elliptical in a counter-clockwise (retrograde) direction on the surface (Fig. 1). It will change to prograde in a certain depth. The motion is constrained to the vertical plane consistent with the direction of wave propagation (Babuska & Cara, 1991, p. 30). Longer wavelengths penetrate deeper than shorter wavelengths for a given mode, in general exhibit greater phase velocities, and are more sensitive to the elastic properties of the deeper layers (Babuska & Cara, 1991, p. 30). Shorter wavelengths are sensitive to the physical properties of surface layers. For this reason, a particular mode of surface waves will possess a unique phase velocity for each unique wavelength, leading to dispersion of the seismic signal. Because of dispersion ($dV/df \neq 0$), where V is phase velocity, f is frequency, the phase velocity V (the velocity of any given phase or a wave of single frequency) differs from the group velocity U (the velocity with which the energy in a wavetrain travels). The relationship between the phase velocity and the group velocity is $U = V + f(dV/df)$ (Sheriff, 1991, p. 144).

The S-wave velocity can be derived from inverting the phase velocity of the surface (Rayleigh and/or Love) wave (Dorman & Ewing, 1962). For the case of a solid homogeneous half-space, the Rayleigh wave travels with a velocity of approximately $0{\cdot}9194v_s$, where v_s is the S-wave velocity in the half-space (Sheriff & Geldart, 1983, vol. 1, p. 49) and is not dispersive. In the case of one layer on top of a solid homogeneous half-space, dispersion of the Ray-

Manuscript received 16 December 2002; revised manuscript accepted 8 October 2003.
Discussion on this paper closes 1 July 2004, for further details see p. ii.
* Kansas Geological Survey, The University of Kansas, Lawrence, USA.
† Department of Geophysics, China University of Geosciences, Hubei, P.R. China.
‡ Earth Resources Technology, Inc., Jessup, USA.
§ Calvert Cliffs Nuclear Power Plant, Lusby, USA.

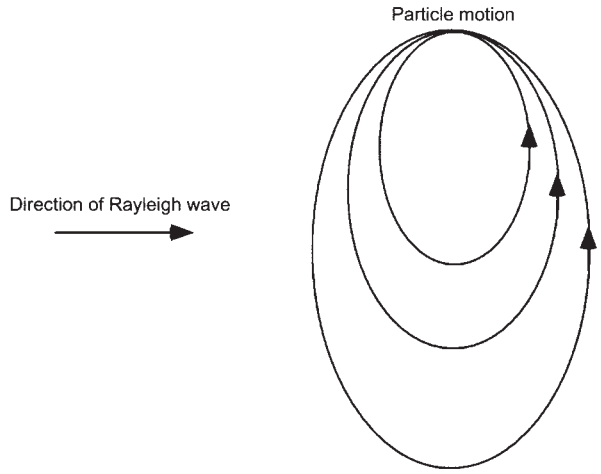

Fig. 1. The particle motion of a Rayleigh wave in a homogeneous medium

leigh wave occurs when the wavelengths of the Rayleigh wave are in the range of 1–30 times the layer thickness (Stokoe *et al.*, 1994). Stokoe *et al.* (1994) also showed that the Rayleigh wave travels with a velocity of approximately $0{\cdot}9194v_1$, where v_1 is the S-wave velocity of the layer, when the wavelengths of the Rayleigh wave are shorter than the layer thickness (Fig. 2(a)). For wavelengths longer than 30 times the layer thickness the Rayleigh wave phase velocity is approximately equal to $0{\cdot}9194v_2$, where v_2 is the S-wave velocity of the half-space (Fig. 2(b)).

Ground roll is a particular type of Rayleigh wave that travels along or near the ground surface and is usually characterised by relatively low velocity, low frequency, and high amplitude (Sheriff, 1991, p. 143). Stokoe & Nazarian (1983) and Nazarian *et al.* (1983) presented a surface-wave method, *spectral analysis of surface waves* (SASW), which analyses the dispersion curve of ground roll to produce near-surface S-wave velocity profiles. Matthews *et al.* (1996) summarised the SASW method and the *continuous surface wave* (CSW) method (Abbiss, 1981; Tokimatsu *et al.*, 1991) with detailed diagrams. SASW has been widely applied to many engineering projects (Sanchez-Salinero *et al.*, 1987; Sheu *et al.*, 1988; Stokoe *et al.*, 1989; Gucunski & Wood, 1991; Hiltunen, 1991; Stokoe *et al.*, 1994).

Inversion of dispersion curves to estimate S-wave velocities deep within the earth was first attempted by Dorman & Ewing (1962). Song *et al.* (1989) related the sensitivity of model parameters to several key parameters by modelling

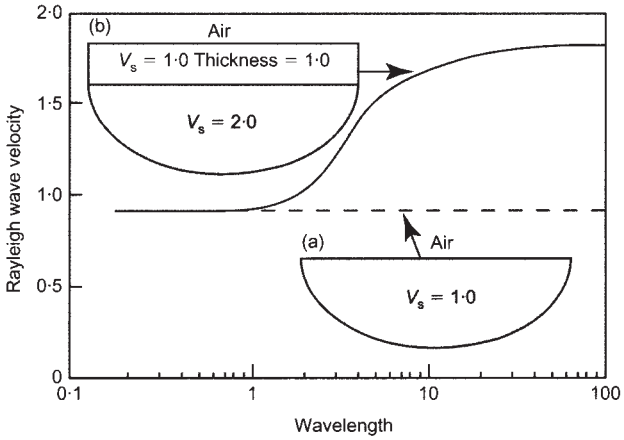

Fig. 2. Rayleigh wave phase velocity against wavelength in: (a) a homogeneous half-space; (b) a softer layer over a stiffer half-space (from Stokoe *et al.*, 1994)

and presentation of two real examples where surface waves were used to obtain S-wave velocities. Turner (1990) examined the feasibility of inverting surface waves (Rayleigh and Love) to estimate S-wave and P-wave velocities, and concluded that it is difficult to obtain P-wave velocities from surface waves. Dispersion curves are inverted for S-wave velocities using least-squares techniques in the SASW method (Nazarian *et al.*, 1983; Stokoe & Nazarian, 1983). Rix & Leipski (1991) examined the influence of the number of dispersion data, the maximum wavelength, and distribution of dispersion data with wavelength on the accuracy and resolution of S-wave velocity profiles.

Matthews *et al.* (1996) categorised surface wave inversion techniques into three groups: the wavelength–depth method, Haskell–Thomson matrix techniques (Haskell, 1953), and finite element approaches. The wavelength–depth method is the simplest, but least exact (Matthews *et al.*, 1996). This method is based on the fact that the amplitude of a Rayleigh wave diminishes at a certain depth. The phase velocity of the Rayleigh wave is converted into an S-wave velocity using empirical formulae (e.g. Jones, 1958; Abbiss, 1981;) at a depth related to the wavelength of the Rayleigh wave. Haskell (1953) derived a matrix formula to calculate the dispersion of Rayleigh waves in multilayered media. Inversion algorithms with the forward calculation based on the Haskell matrix are called Haskell–Thomson matrix techniques. Stokoe and his co-workers used this method in their research (e.g. Nazarian *et al.*, 1983; Stokoe & Nazarian, 1983; Sanchez-Salinero *et al.*, 1987; Sheu *et al.*, 1988; Stokoe *et al.*, 1989, 1994; Rix & Leipski, 1991). Finite element techniques calculate dispersion curves using dynamic finite elements (e.g. Bathe, 1982). These techniques can be used to solve complex subsurface geometries, but they are time consuming.

A research project under way since 1995 at the Kansas Geological Survey estimated S-wave velocity from ground roll. The fundamental methodology for *multichannel analysis of surface waves* (MASW) can be found in Park *et al.* (1999a) and Xia *et al.* (1999). Surface wave energy on a multichannel record can be easily distinguished and extracted with much less interference from body waves. Dispersion images with higher resolution can be obtained by a phase-shifting method (Park *et al.*, 1998) than from an F–K transformation method (McMechan & Yedlin, 1981). It is critical to determine 'good' initial estimates to ensure inversion convergence. An inversion algorithm developed by Xia *et al.* (1999) started with a group of initial S-wave estimates that were determined by empirical formulae based on modelling results. Forward calculation of dispersion curves in their algorithm is based on the Haskell–Thomson matrix (Haskell, 1953). An iterative solution (Xia *et al.*, 1999) to the weighted inverse problem proved very effective in the high-frequency range when using the Levenberg–Marquardt (Levenberg, 1944; Marquardt, 1963) and singular value decomposition techniques (Golub & Reinsch, 1970). Convergence of the weighted solution is guaranteed through selection of the damping factor using the Levenberg–Marquardt method. An algorithm for fast estimation of S-wave velocity from Rayleigh waves for a compressible Gibson half-space (shear modulus varies linearly with depth) was also developed (Xia *et al.*, 1997). Based on Xia *et al.*'s report (2000a), the fundamental-mode phase velocities, when calculated with high accuracy, can generally provide reliable S-wave velocities (±15%) in unconsolidated sediments. Xia *et al.* (2002a) compared S-wave velocity profiles inverted from fundamental-mode phase velocities of surface waves with borehole measurements, and confirmed that reliable S-wave velocities (±15%) can be derived from surface wave techniques. Xia *et al.* (2003) concluded that the accuracy of

S-wave velocity and the resolution of inverted model can be increased if higher modes of surface waves are available and included in the inversion process. Recent advances in the use of surface waves for near-surface imaging incorporated the MASW method (Park *et al.*, 1996, 1999a, 1999b; Xia *et al.*, 2000a, 2002a, 2002b, 2003) with a standard common depth point (CDP) roll-along acquisition format (Mayne, 1962) similar to conventional petroleum exploration data acquisition. The CDP roll-along acquisition method is a recording method whereby each source is recorded at a number of receiver locations, and each receiver location is used to record from a number of source locations (Sheriff, 1991, p. 45). Combining these two uniquely different approaches to acoustic imaging of the subsurface allows high confidence, non-invasive delineation of horizontal and vertical variations in near-surface material properties (Xia *et al.*, 1998, 2000b; Miller *et al.*, 1999).

A collapse developed in the Tank Farm area at Calvert Cliffs Nuclear Power Plant, Maryland, in early 2001 (Fig. 3(a)). Sediments of the Chesapeake Group of Miocene age underlie the plant area to a depth of about 60 m. The material in this group consists of essentially horizontally stratified sandy and clayey silt with occasional interbeds of sand and shells. The power plant foundations were built after excavation. Original material was backfilled and then used to raise the ground surface to +13·5 m. The original backfill was starting from 18 m below the present ground surface. The backfilled material was free of vegetation, organic material, soil with doubtful bearing or settlement characteristics, and rock or rock-like particles in excess of 4 in (100 mm). Additionally, this material had a compaction requirement of 95% compaction based on standard Proctor (ASTM D-698 or AASHO T-99) and a moisture content less than 4%. To prevent damage to nearby structures, the collapse was quickly filled with uncompacted mixture of coarse sand (80% with grain size ~4·76 mm), silt (9% with grain size ~0·074 mm) and gravel (10% with grain size ~10 mm and 1% with grain size ~20 mm). Total filling is approximately 36 000 kg. However, the plant had an immediate need to determine whether more underground voids existed.

The collapse was next to the subsurface drain system (SSD). The SSD piping (Fig. 3(b)) was installed during this backfill work. The subsurface drain system is designed to lower the local water table from approximately +6 m above bay level to +3 m. The location of the collapse was over an SSD pipe buried at an elevation of +0·9 m (reference is to Chesapeake Bay level). The ground surface in the collapse area is +13·5 m. The subsurface drain system is connected vertically into the top of the condenser cooling water discharge conduit at an elevation of −1·2 m. The collapse was located approximately 4·5 m horizontally from this connection to the conduit. The static pressure in the conduit forces saltwater up into the corrugated metal subsurface drain pipe. Because the conduit discharges to the Chesapeake Bay, this static pressure varies with the tide. The collapsed section of pipe was in the tidal zone. The tidal action (inflow/outflow) and groundwater flow caused soil to be removed from the area around the collapsed pipe. The discharge conduit is a monolithic concrete structure 18·3 m wide, 6 m tall (a rectangular cross-section) and approximately 240 m long. The top of the discharge conduit (on the left side of Fig. 3(b)) is approximately 14·7 m below the ground surface. The discharge conduit is horizontally divided into four separate tunnels, each approximately 3·6 m by 3·6 m in dimension. Each tunnel carries a cooling water flow of 2·27 Ml/min (total flow in the conduit is 9·08 Ml/min).

The area potentially affected by the collapse needs to be defined to prevent further damage and ensure the safety of the plant. Voids can be difficult to detect from surface investigations, and can be expensive to detect with hit and miss drilling. The turbines and transformers of the power plant were running during data acquisition, which generated a noise level 50–100 times higher than the noise level for a normal shallow high-resolution reflection/refraction survey. The surface-wave method was proposed to define the zone affected by the collapse because it was hoped that changes in shear wave velocity might be expected at the boundary between unconsolidated materials and consolidated bedrock as well as unconsolidated and fill materials. This study will focus on the following goals and objectives: feasibility of defining a zone affected by the collapse at least 15 m deep in the noisy environment by using the MASW method with fundamental mode data acquired with the standard CDP roll-along acquisition format and evaluation of effective imaging of S-wave velocity fields.

THE METHOD

Surface-wave imaging has shown great promise for detecting shallow tunnels (Xia *et al.*, 1998) and bedrock surfaces (Miller *et al.*, 1999; Xia *et al.*, 2000b). Extension of this imaging technology to include lateral variations in lithology has required a unique approach incorporating MASW and CDP methods. Integrating these techniques provides a two-dimensional continuous shear wave velocity profile of the subsurface. Signal enhancement resulting from determination of a dispersion curve using upwards of 60 closely spaced receiving channels and the calculation of a dispersion curve every 0·6 m or so along the ground surface provides a unique, relatively continuous view of the shallow subsurface. This highly redundant method enhances the accuracy of the calculated shear wave velocity and minimises the likelihood that the irregularities associated with an occasional erratic dispersion curve will corrupt the data analysis.

The MASW method is based on the fact that the S-wave velocity is the dominant influence on Rayleigh wave velocities for a layered earth model, which assures us that inverting phase velocities will give us an S-wave velocity profile (one-dimensional S-wave velocity function, V_S against depth) at the centre of a receiver spread. Because data are acquired in the standard CDP format, phase velocities of ground roll can be extracted from each shot gather (a side-by-side stored number of seismic traces that have the same seismic source) so that numerous one-dimensional S-wave profiles along a survey line can generated. A two-dimensional vertical section of S-wave velocity can be generated by any contouring software.

A number of multichannel records should first be collected in the standard CDP roll-along acquisition format. If a swept source (vibroseis—the frequency is varied continuously during a 'sweep' period) is used, the recorded data should be converted into a correlated format, which is equivalent to data acquired with an impulsive source. Surface impact sources and receivers with a low response frequency, normally less than 8 Hz, should be chosen to acquire surface-wave data. Data acquisition parameters, such as source–receiver offset and receiver spacing, should be set to enhance ground-roll signals (Park *et al.*, 1999a).

Once the data collection is completed, phase velocities (dispersion curves) of the ground roll of each shot gather should be calculated. The frequency range and phase velocity range of the ground roll need to be determined by analysing data along the entire line. These two ranges are very important constraints to correctly extract the dispersion curve from each shot gather. They not only help to eliminate noise such as body waves or the higher mode of Rayleigh waves during calculation of phase velocities (Park *et al.*,

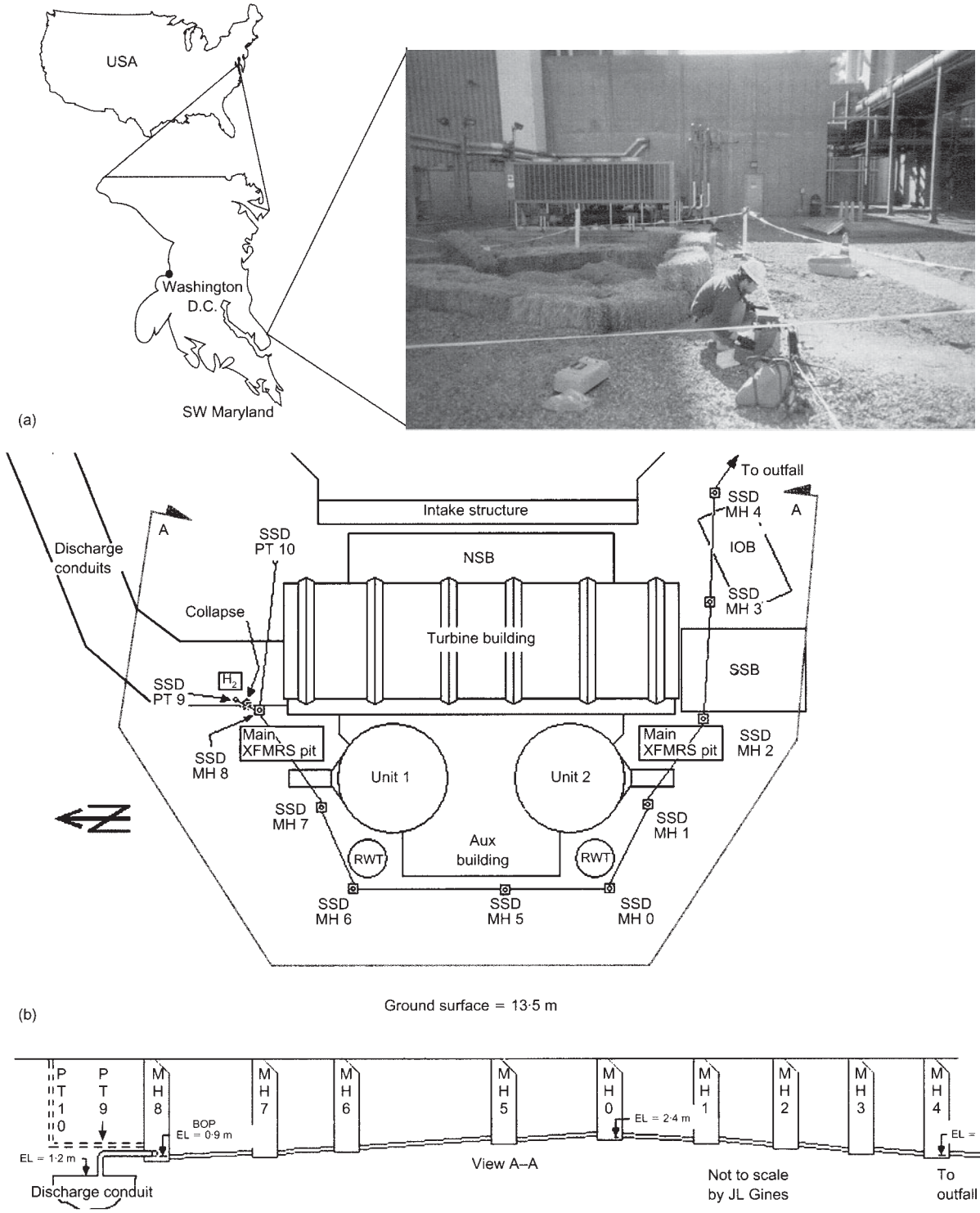

Fig. 3. (a) Collapse surrounded by straw bales at Calvert Cliffs Nuclear Power Plant, Calvert County, MD. A geophysicist of Earth Resources Technology, Inc. was operating a seismograph. The structure at the back of the photo is the turbine building. The transformer is located to the right in the photo. Two turbines and the transformer were running during surface wave data acquisition. The groundwater drainage system is shown in (b) with the collapse between SSD PT9 and SSD MH8

1999a), but also assist in defining the thickness of the layer model.

Inversion should be performed on each dispersion curve to generate a profile of S-wave velocity against depth (Xia *et al.*, 1999). The inverted S-wave velocity profile should be located in the middle of the receiver spread (Miller & Xia, 1999). Initial models are a key factor to ensure convergence of the inversion process. After processing more than 5000 shots of real data and countless sets of modelling data, initial models defined by Xia *et al.*'s (1999) algorithm are generally converged to models that are acceptable in geology (agreement with geological model) and also fit the dispersion curve in a given error range. In our experience layers should be chosen between 5 and 20 for the model in order to achieve good agreement with groundtruth, based on the accuracy of surface-wave data, investigation depths, and required resolution of S-wave velocity. The thickness of each layer varies based on the depths of interest. For example, for

a geological problem with a depth of interest of 15 m, a 10-layer model is normally chosen with the first three layers being 0·9 m thick, the next three layers 1·8 m thick, the last three layers 3 m thick, and a half-space. The thickness of a layer varies with accuracy of dispersion curves. A trade-off between the resolution of a model (layer thickness) and errors in the model must be made according to the accuracy of the dispersion curves. The thickness of layers is a critical parameter for the inversion processing to converge to a smooth solution (Xia *et al.*, 2003). The inverted S-wave velocity profile for each shot gather is the result of horizontally averaging across the length of the receiver spread.

Gridding algorithms, such as kriging or minimum curvature, may be used to generate a two-dimensional contour map of the S-wave velocity of a vertical section. With density information, a shear modulus section can be generated simultaneously. Two-dimensional data processing techniques, such as regression analysis, can be easily applied to a vertical section of S-wave velocity to enhance local anomalies.

On a two-dimensional S-wave velocity map the bedrock surface is usually associated with high S-wave velocity gradients, whereas fracture zones, voids, buried landfill edges and the like may be indicated by S-wave anomalies such as low-velocity zones. The general procedure for generating a two-dimensional S-wave velocity map is summarised as follows (Fig. 4).

(*a*) collection of a number of multichannel records in a standard CDP roll-along acquisition format; the field data acquisition parameters are chosen to enhance broadband ground roll
(*b*) calculation of the phase velocity of the ground roll of each shot gather once the data collection is completed
(*c*) inversion of the phase velocity to generate a profile of S-wave velocity against depth that is located at the centre of the receiver spread steps (a) to (c) are repeated to generate a number of S-wave velocity profiles when a seismic source is moved along a line)
(*d*) generation of a two-dimensional contour map of the S-wave velocity of a vertical section.

Because each shot gather covers a certain horizontal length, the S-wave velocity profile is an average result of the subsurface covered by that length. It is clear that a two-dimensional S-wave velocity section generated by the method described will possess smear effects, so the two-dimensional S-wave velocity section generated by the method is a smoothed (or low-resolution) version of a subsurface S-wave velocity section. It is certainly possible that interpretation based on the smoothed results will miss some low-amplitude and/or high-frequency anomalies. Improved resolution of a two-dimensional velocity section is a current topic of research and will be addressed in the near future.

DATA ACQUISITION

Parameters for surface wave data acquisition are different from a shallow reflection and/or refraction survey and critical to successfully conducting a surface wave survey. They are

(*a*) the nearest source–receiver offset (A, see Fig. 5)
(*b*) receiver spacing (B)
(*c*) receiver spread—distance between the first receiver and the last receiver (C).

The nearest source–receiver offset should be determined by minimising near-offset effects (Park *et al.*, 1999a). Near-offset effects occur when lower frequency components are not fully developed as plane waves. Plane-wave propagation of surface waves occurs when the nearest source–receiver offset is greater than half the maximum desired wavelength. The maximum desired wavelength is about equal to the maximum investigation depth, so that the nearest source–receiver offset is about equal to half the maximum investigation depth. Receiver spacing should follow the Nyquist sampling theorem (Sheriff & Geldart, 1983, vol. 2, pp. 29–31). Receiver spacing determines the shortest wavelength in recorded data, which is a guideline for determining the thickness of a layer model, and is also a limit in the inverted S-wave velocity model. Receiver spread should also follow the Nyquist sampling theorem. Receiver spread determines the longest wavelength in the recorded data, which is a guideline for determining the total thickness of layers on the top of the half-space. The receiver spread is limited by far-offset effects that occur when higher-frequency components of surface waves are contaminated by body waves due to attenuation of high-frequency components of surface waves.

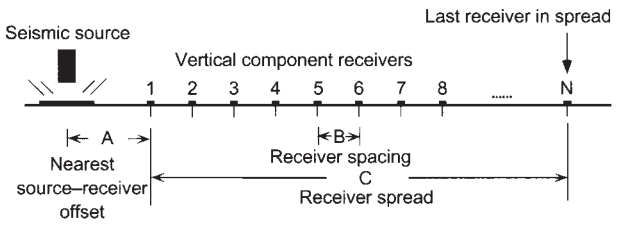

Fig. 5. Surface wave data acquisition parameters

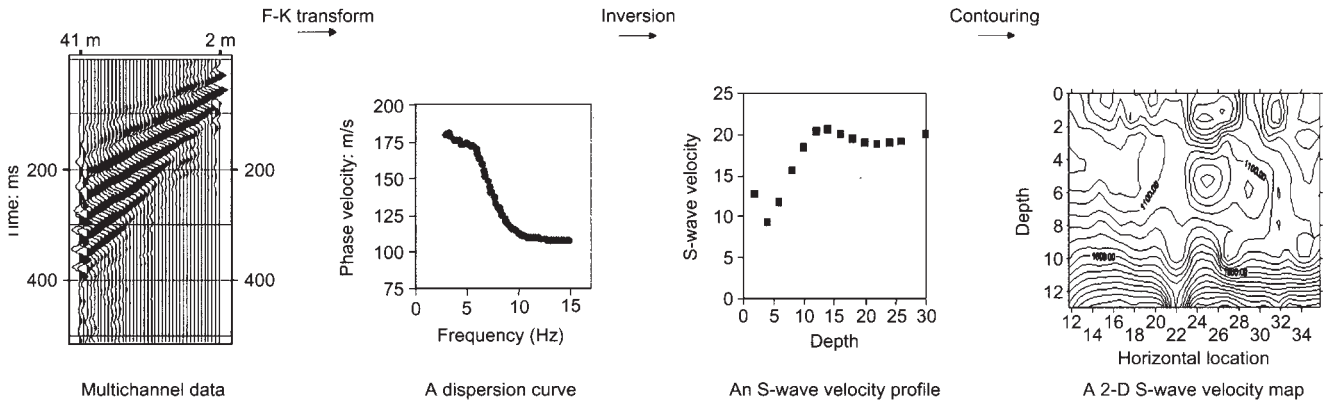

Fig. 4. Construction of two-dimensional S-wave velocity map by the MASW method. Rayleigh wave phase velocities are extracted from the field data in the F–K domain. Phase velocities are inverted for a shear-wave velocity profile (V_s against depth). After a number of S-wave velocity profiles are generated when a seismic source is moving along a line, finally, a two-dimensional S-wave velocity map is generated with contouring software

The evidence of the contamination is that the linearity of high-frequency components of surface waves no longer exists. An example of far-offset effects can be found in Park *et al.*'s work (Park *et al.*, 1999a).

Because the depth to the drainage tunnel is 13·5 m, the investigation depth for this project was approximately 15 m. The nearest source–receiver offset is chosen as half the investigation depth, in this case 7·2 m. With a 24-channel recording system, the receiver spread is critical to maintain the proper resolution in the frequency–velocity domain, thereby allowing the software to accurately pick phase velocities of surface waves. The half wavelength is the effective penetrating depth of surface waves. In this project, we need to record a 30 m wavelength component of surface waves. In accordance with the availability of data acquisition instruments, this condition determined that the best receiver spread was 27·6 m with a receiver interval of 1·2 m.

Data were collected using a 24-channel StrataView seismograph with a 5·5 kg hammer and a 0·3 m × 0·3 m aluminium plate as the seismic source in a standard CDP roll-along acquisition format to generate S-wave velocity sections. Twenty-four 4·5 Hz (natural frequency) vertical-component geophones (with plates) were deployed on the same geophone interval 1·2 m with 7·2 m from the source to the nearest geophone along five lines (Fig. 6). Six impacts at each shot station were vertically stacked—summing seismic data in the time domain—to increase the signal-to-noise ratio.

Five lines were designed around the collapse based on accessibility (Fig. 6), and 137 shots of surface-wave data were collected along those lines. Data were acquired along asphalt or concrete roads and in a gravel-paved yard. Total line length of the surface-wave survey was 330 m. Total imaging length of the five lines was 157 m. The data were acquired in an extremely noisy environment. The noise level was 50–100 times higher than the noise level for a normal shallow high-resolution reflection/refraction survey. At this noise level, it is extremely difficult to acquire meaningful body-wave seismic data.

DATA PROCESSING

Data were processed by WinSeis© and SurfSeis©, programs developed at the Kansas Geological Survey. A pre-processing flow of the surface-wave data running with WinSeis© included bandpass filtering (a trapezoid with four frequencies of 3, 6, 40 and 60 Hz), automatic gain control scaling (AGC) with a time window of 100 ms, and F–K filtering (a filtered pie defined by two lines with slopes of −3 ms/trace and −9 ms/trace respectively). The bandpass filter and AGC were used to filter unwanted frequency components (mostly body waves) and to balance the surface-wave spectrum respectively. The F–K filter was employed to suppress noise from the turbine and transformer from the end of a line (Figs 7(a) and 7(b)). Rayleigh wave energy is clearly shown in the frequency–velocity domain (Fig. 7(c)) even though it is difficult to identify it in the time–space domain (Figs 7a and 7b). Phase velocities of the fundamental mode—shown by a white line (Fig. 7(c))—associated with the maximum of energy at each frequency can be automatically picked up by SurfSeis©. It is crucial to recognise the correct pattern of the fundamental mode of a dispersion curve. Energy around 30–50 Hz with velocities from 300 to 750 m/s is probably due to a higher mode of

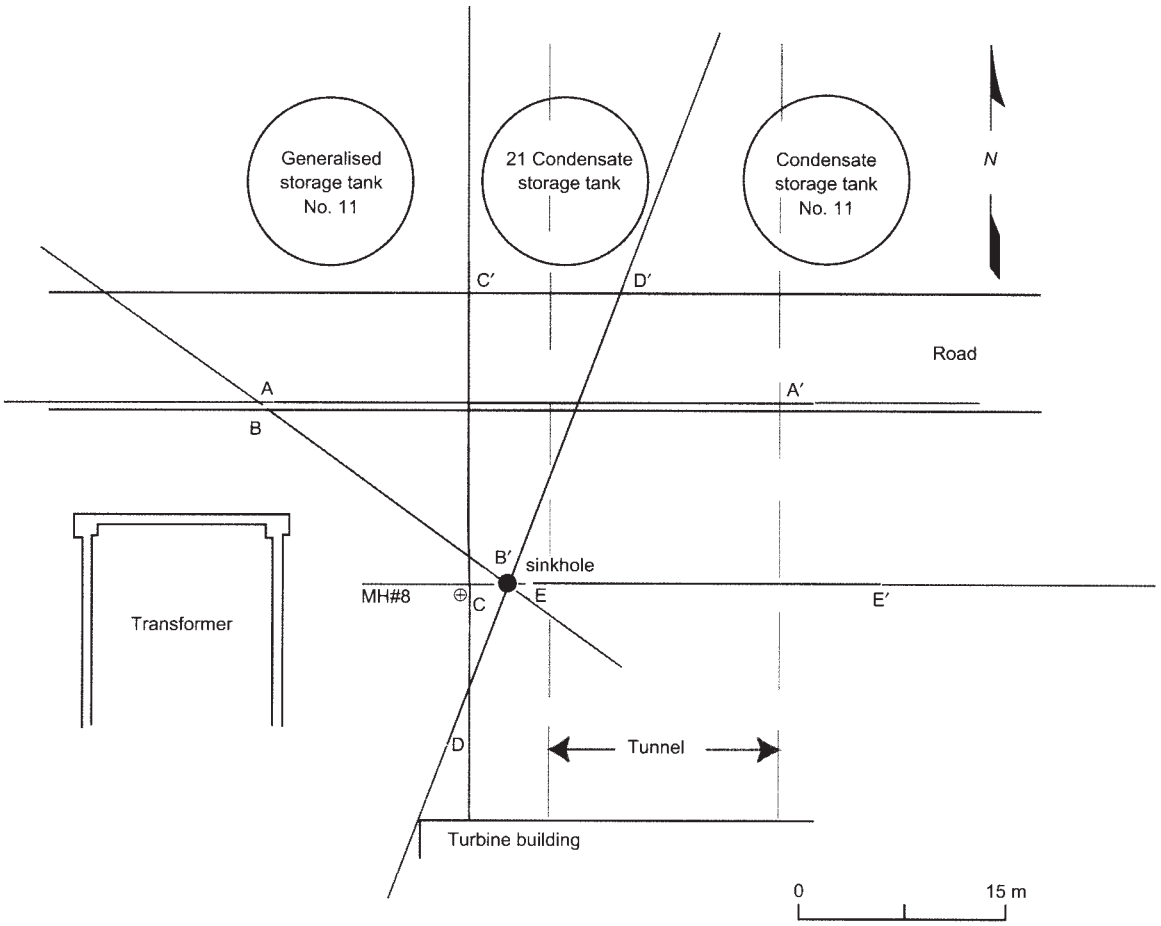

Fig. 6. Location of surface-wave seismic lines. The beginning and end of the image along lines are indicated by letters

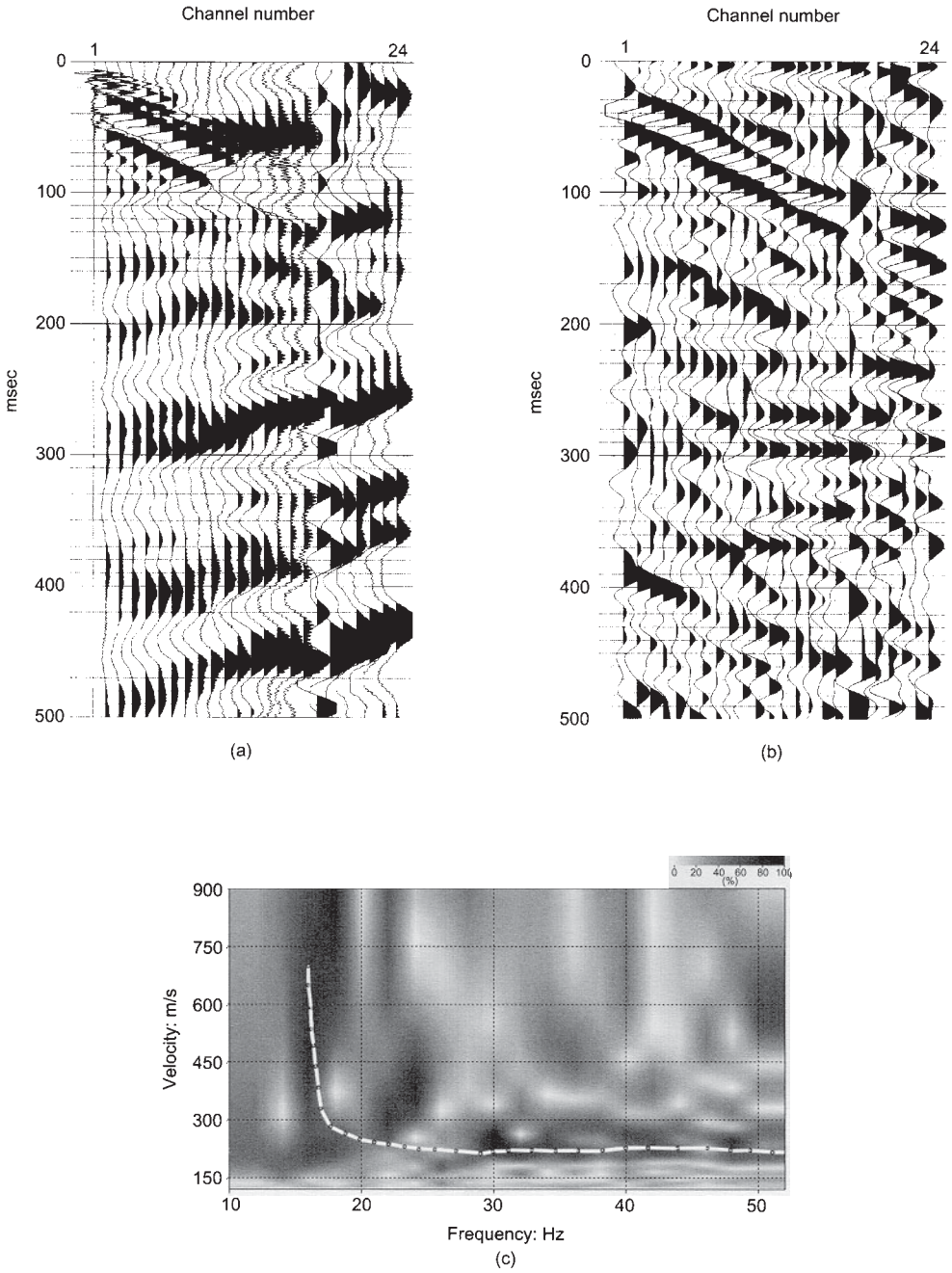

Fig. 7. Example of field shot gather: (a) raw data; (b) data after a bandpass filtering, an AGC scaling, and an F–K filtering; (c) phase velocities (solid line with dots) on top of seismic image of shot gather (b) in frequency–velocity domain

Rayleigh waves. Also, energy around 50 Hz with velocity about 600 m/s is most likely due to body waves.

Dispersion curves were generated from the time domain data using SurfSeis© mainly from 13 Hz to 27 Hz for all shots. Wavelengths of surface waves ranged from 7·5 m to 72 m. A five-layer model, with thicknesses of 3 m, 3 m, 4·5 m, 4·5 m, and the half-space, was chosen during inversion processing. The layer thickness of the model should be controlled by the shortest wavelength of the surface waves. This relatively low-resolution model was chosen to stabilise the inversion processing (Xia *et al.*, 2003) because of extremely noisy data.

Phase velocities of surface waves were inverted into S-wave velocities of the layered earth model for each shot. The inverted S-wave velocity profile was placed at the centre of a receiver spread of each shot gather. The contouring software Surfer© was finally used to generate two-dimensional S-wave velocity fields (Figs 8–11) of each line.

DATA INTERPRETATION

Interpretation of S-wave velocity fields is straightforward. Relative lower S-wave velocities in the vicinity of the collapse clearly delineated a possible zone affected by the collapse. Relative higher S-wave velocities indicated the location of the water tunnels.

Zone affected by collapse

The collapse was filled by an uncompacted mixture of sand and gravel to prevent additional damage. Although the refilling reduced the velocity contrast in the zone affected by

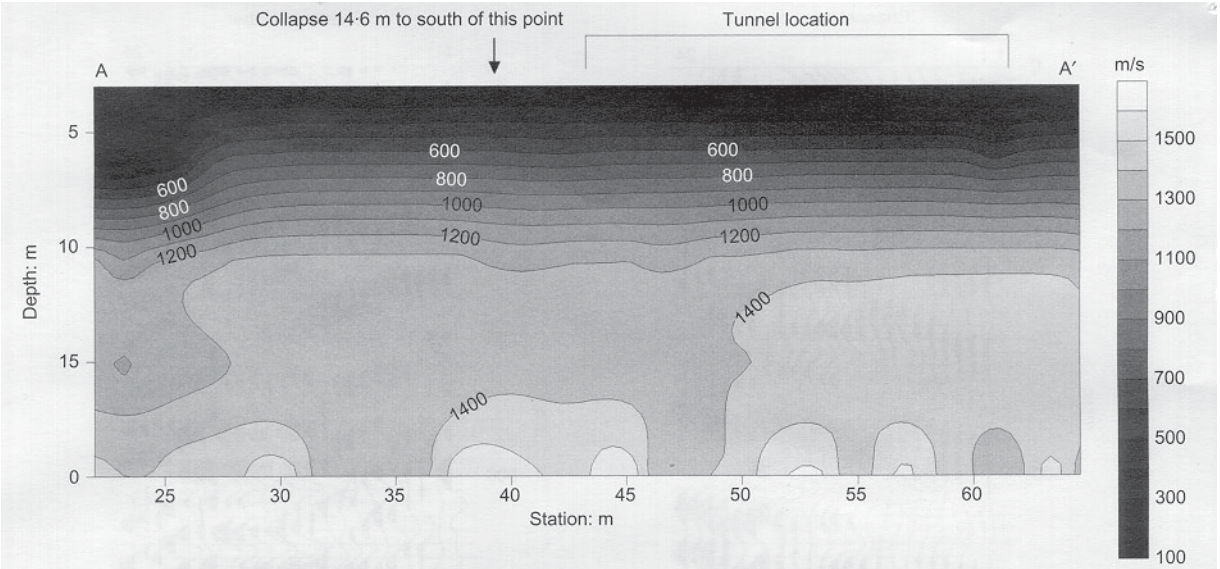

Fig. 8. S-wave velocity field of line A–A′. A contour interval is 100 m/s

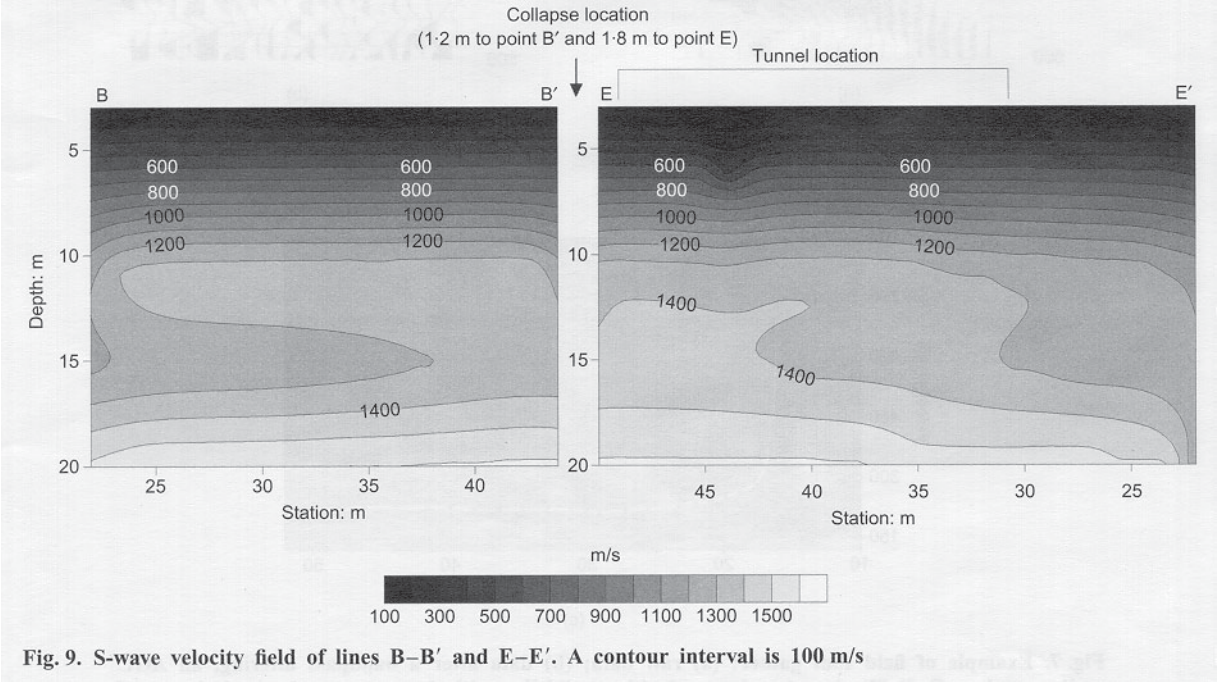

Fig. 9. S-wave velocity field of lines B–B′ and E–E′. A contour interval is 100 m/s

the collapse, we expect that the uncompacted mixture of sand and gravel is much less compacted than the surrounding materials, so the zone affected by the collapse will still show anomalies, with a lower S-wave velocity. An imaging point of the surface-wave method is located in the centre of the receiver spread of each shot (Miller & Xia, 1999). Because of the limited access to the area surrounding the collapse, only line D–D′ (Fig. 11) contains imaging points that traverse the collapse. The collapse was located at station 47 of line D–D′. A striking relative lower S-wave velocity field from stations 46 to 52 below 12 m of depth is shown in Fig. 11. Based on its low S-wave velocity, it is likely that the area that possesses lower S-wave velocity along line D–D′ was due to the collapse. It is also interesting to see that the collapse was located at station 47 instead of 49, the centre of the affected area. This might be due to the smear effect of S-wave velocities at deeper depths. The water tunnel located approximately at station 37 and less on line D–D′ showed a higher S-wave velocity. This tunnel might cause a slight shift in the affected area of our interpretation of the S-wave velocity field.

Line A–A′ (Fig. 8) possesses a relatively lower S-wave velocity field around station 34, similar to that shown for station 47 of line D–D′ around the collapse. A chimney-shaped S-wave velocity field from stations 31 to 37 below 12 m of depth indicates a possible area affected by the collapse. We suggest that the zone affected by the collapse extends northward at least to line A–A′. The north–south line C–C′ seems to support this suggestion.

The S-wave velocity field of line C–C′ (Fig. 10) presents an anomalous low that covers the entire line at a depth of 12–15 m. This anomaly reveals a possible zone affected by the collapse along line C–C′. These results indicate that the chimney-shaped anomaly shown on line A–A′ was most likely related to the collapse. Based on previous interpretation of low S-wave velocity anomalies, a possible zone affected by the collapse has been delineated even with the limited accessibility and the limited resolution of S-wave

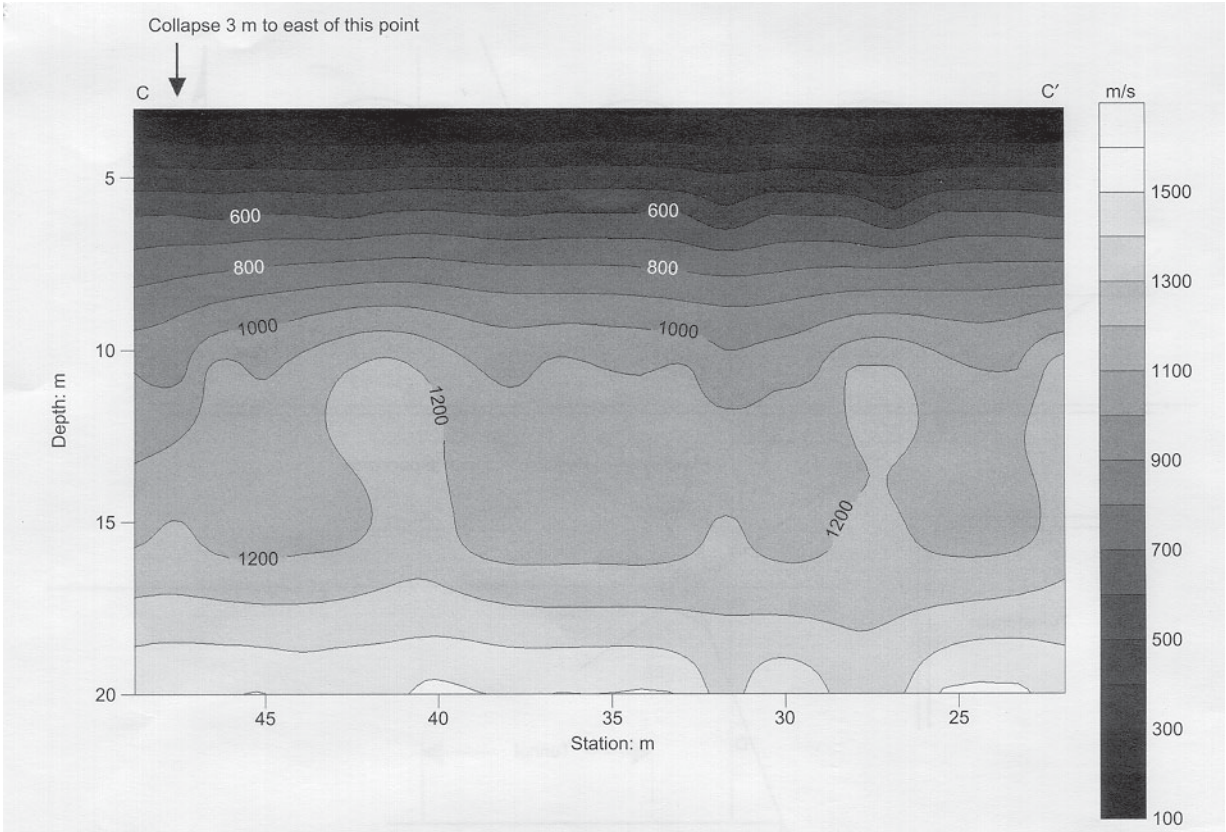

Fig. 10. S-wave velocity field of line C–C′. A contour interval is 100 m/s

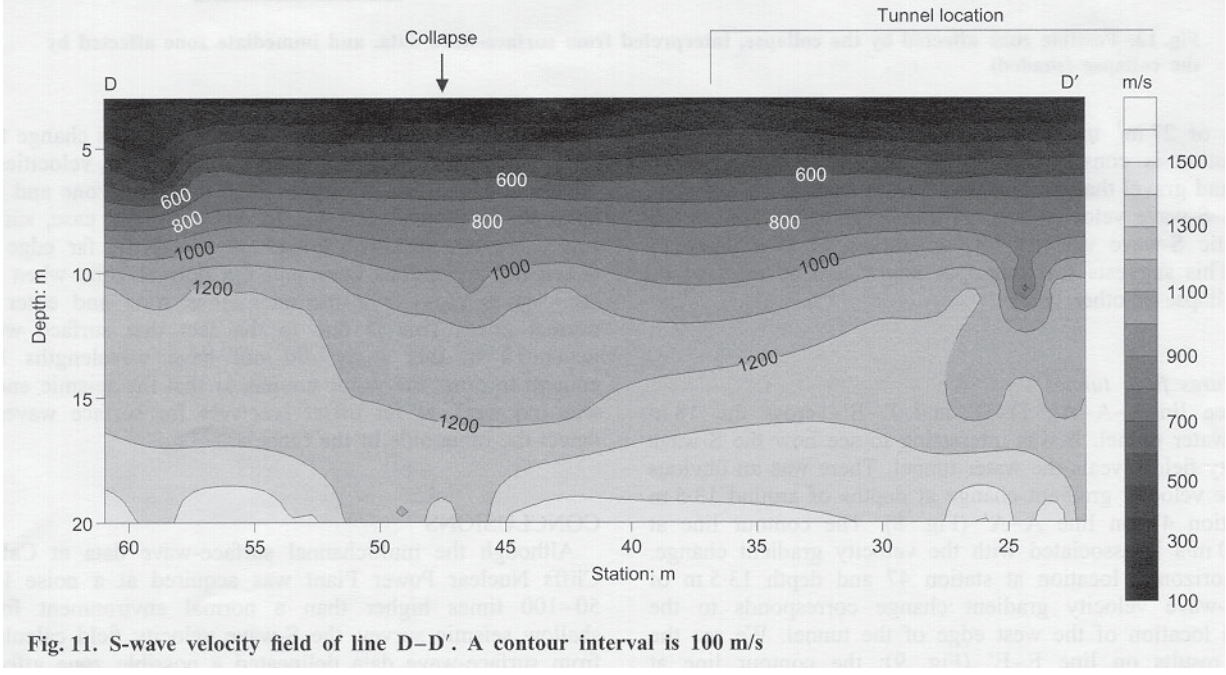

Fig. 11. S-wave velocity field of line D–D′. A contour interval is 100 m/s

velocity fields. The ground affected by the collapse is shown in Fig. 12 based on surface wave data. The potential zone affected by the collapse covered most of the part of line C–C′ that was between lines A–A′ and E–E′. The area was approximately 18 m long and 6 m wide. The depth of the potential affected volume was at 12–15 m.

According to the amount of sand and gravel required to fill the collapse (36 000 kg), the volume of the void immediately associated with the collapse is estimated to be around 26 m^3 (assuming a density of the uncompacted sand and gravel of 1400 kg/m^3). The volume of the void will be larger than 26 m^3 if the uncompacted sand and gravel density is less than 1400 kg/m^3. The low S-wave velocity zone at depths of 12–15 m along line C–C′ (Fig. 10) suggests that the vertical dimension affected is around 13 m. We also see that the affected lengths along both lines A–A′ (31 to 36) and D–D′ (46 to 51) are around 5 m. Thus, in our interpretation, a northeast–southwest measurement for the zone affected by the collapse is approximately 5 m, assuming the affected area is approximately rectangular. These results suggest that the immediately affected volume after uncompacted sand and gravel filling is a symmetrical cube 3 m in

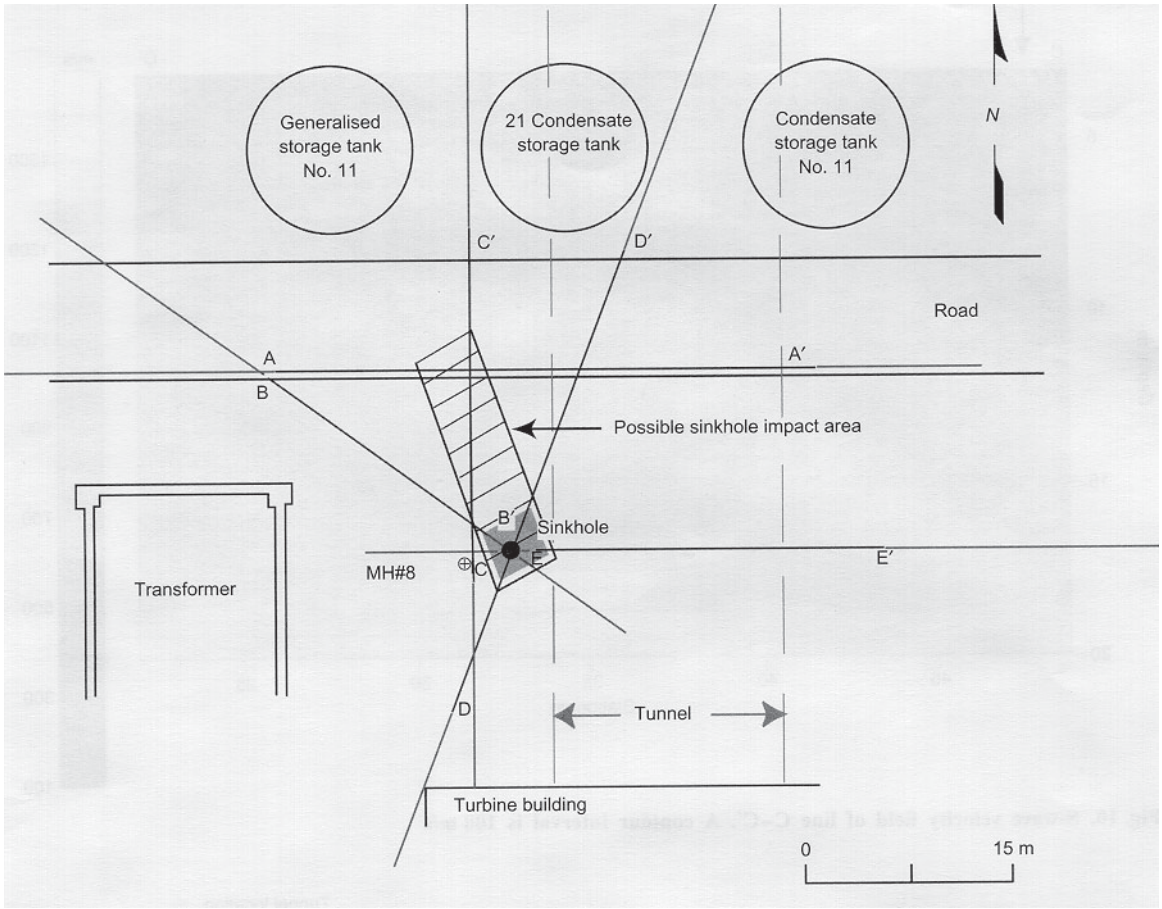

Fig. 12. Possible zone affected by the collapse, interpreted from surface-wave data, and immediate zone affected by the collapse (shaded)

length or 27 m^3 in volume (shaded area in Fig. 12). This calculation is consistent with the amount of uncompacted sand and gravel that was used to fill the void.

The S-wave velocity field of line E–E′ (Fig. 9) shows a dramatic S-wave velocity low at station 44 at a depth of 6 m. This suggests that this spot might also be affected by the collapse or other voids.

Signatures from tunnel

Three lines—A–A′, D–D′ and E–E′—cross the 18 m wide water tunnel. It was interesting to see how the S-wave velocity field reveals the water tunnel. There was an obvious S-wave velocity gradient change at depths of around 13·5 m at station 47 on line A–A′ (Fig. 8). The contour line at ~1400 m/s is associated with the velocity gradient change. The horizontal location at station 47 and depth 13·5 m of the S-wave velocity gradient change corresponds to the spatial location of the west edge of the tunnel. We see the same results on line E–E′ (Fig. 9); the contour line at 1300 m/s is associated with the S-wave velocity gradient change and suggests the east edge of the tunnel. That the tunnel was revealed by the contour lines with different velocity values provides an indication of the resolution of the surface-wave method in this environmental setting. Because of the noise level, the difference of 100 m/s in S-wave velocity maps did not surprise us.

It is worthy of note that the S-wave velocity field reveals only one side of the tunnel. Based on the data-acquisition geometry, the source was on the west side of the receiver spread for line A–A′ and on the east side of the receiver spread for line E–E′. The data-acquisition geometry and S-wave velocity field suggest that surface waves change their behaviour significantly in response to S-wave velocities of materials when they propagate from a normal zone and then cross to an anomalous zone. In this particular case, surface waves are not sensitive enough to reveal the far edge between the anomalous zone and the normal zone when surface waves cross over the anomalous zone and enter the normal zone. This is due to the fact that surface waves generated in this study did not have wavelengths long enough to cross the water tunnels or that the seismic energy was too weak at far offset receivers for surface waves to detect the other side of the tunnels.

CONCLUSIONS

Although the multichannel surface-wave data at Calvert Cliffs Nuclear Power Plant was acquired at a noise level 50–100 times higher than a normal environment for a shallow seismic survey, the S-wave velocity field calculated from surface-wave data delineated a possible zone affected by the collapse. Depending on the source–receiver geometry, the S-wave velocity field also revealed one side of the water tunnel. This case study shows high potential for applying multichannel surface wave techniques to groundwater, engineering and environmental problems in urban noisy areas.

ACKNOWLEDGEMENTS

We greatly appreciate Mary Brohammer, Janice Sorensen, and Julia Shuklaper for their participation in preparation of this manuscript. We also thank two anonymous reviewers for their constructive and detailed suggestions.

REFERENCES

Abbiss, C .P. (1981). Shear wave measurements of the elasticity of the ground. *Géotechnique* **31**, No. 1, 91–104.

Babuska, V. & Cara, M. (1991). *Seismic anisotropy in the Earth*. Boston: Kluwer Academic.

Bathe, K. J. (1982). *Finite element procedures for engineering analysis*. Englewood Cliffs, NJ: Prentice Hall.

Clayton, C. R. I. (1993), *The standard penetration test (SPT): methods and use*, Funders Report CP/7. London: Construction Industry Research and Information Association.

Clayton, C. R. I., Matthews, M. C. & Simons, N. E. (1995). *Site investigation*. Oxford: Blackwell Science.

Dorman, J. & Ewing, M. (1962). Numerical inversion of seismic surface wave dispersion data and crust-mantle structure in the New York–Pennsylvania area. *J. Geophys. Res.* **67**, 5227–5241.

Golub, G. H. & Reinsch, C. (1970). Singular value decomposition and least-squares solution. *Numerische Mathematik* **14**, 403–420.

Gucunski, N. & Wood, R. D. (1991). Instrumentation for SASW testing. In *Recent advances in instrumentation, data acquisition and testing in soil dynamics* (eds S. K. Bhatia and G. W. Blaney), pp. 1–16. Geotechnical Special Publication No. 29, American Society of Civil Engineers.

Haskell, N. A. (1953). The dispersion of subsurface waves on multilayered media. *Bull. Seismol. Soc. Am.* **43**, No. 1, 17–34.

Hiltunen, D. R. (1991). Nondestructive evaluation of pavement systems by the SASW method. *Geotechnical News* (Vancouver, BC), September, 22–25.

Imai, T. & Tonouchi, K. (1982). Correlation of N-value with S-wave velocity. *Proc. 2nd Eur. Symp. on Penetration Testing, Amsterdam*, 67–72.

Jones, R. B. (1958). In-situ measurement of the dynamic properties of soil by vibration methods. *Géotechnique* **8**, No. 1, 1–21.

Levenberg, K. (1944). A method for the solution of certain non-linear problems in least squares. *Q. Appl. Math.* **2**, 164–168.

Marquardt, D. W. (1963). An algorithm for least squares estimation of nonlinear parameters. *J. Soc. Indust. Appl. Math.* **2**, 431–441.

Matthews, M. C., Hope, V. S. & Clayton, C. R. I. (1996). The use of surface waves in the determination of ground stiffness profiles. *Proc. Instn Civ. Engrs Geotech. Engng* **119**, 84–95.

Mayne, W. H. (1962). Horizontal data stacking techniques. *Geophysics* **27** (suppl.), 927–937.

McMechan, G. A. & Yedlin, M. J. (1981). Analysis of dispersive waves by wave field transformation. *Geophysics* **46**, 869–874.

Miller, R. D. & Xia, J. (1999). Feasibility of seismic techniques to delineate dissolution features in the upper 600 ft at Alabama Electric Cooperative's proposed Damascus site: Interim report, Kansas Geological Survey Open-file Report 99–3. Lawrence, KS: Kansas Geological Survey.

Miller, R. D., Xia, J., Park, C. B. & Ivanov, J. (1999). Multichannel analysis of surface waves to map bedrock. *The Leading Edge* **18**, No. 12, 1392–1396.

Nazarian, S., Stokoe, K. H. II & Hudson, W. R. (1983). Use of spectral analysis of surface waves method for determination of moduli and thicknesses of pavement systems. *Transp. Res. Rec.* No. 930, 38–45.

Park, C. B., Miller, R. D. & Xia, J. (1996). Multi-channel analysis of surface waves using Vibroseis (MASWV). *Expanded Abstracts of 66th Ann Mtng of Society of Exploration Geophysicists, Denver*, 68–71.

Park, C. B., Miller, R. D. & Xia, J. (1998). Imaging dispersion curves of surface waves on multi-channel record. *Expanded Abstracts of 68th Ann Mtng of Society of Exploration Geophysicists, Louisiana*, 1377–1380.

Park, C. B, Miller, R. D. & Xia, J. (1999a). Multi-channel analysis of surface waves. *Geophysics* **64**, No. 3, 800–808.

Park, C. B., Miller, R. D. & Xia, J. (1999b). Multimodal analysis of high frequency surface wave. *Proceedings of the symposium on the application of geophysics to engineering and environmental problems (SAGEEP 99)*, Oakland, pp. 115–122.

Rix, G. J. & Leipski, A. E. (1991). Accuracy and resolution of surface wave inversion: Recent advances in instrumentation, data acquisition and testing in soil dynamics, Geotechnical Special Publication No. 29, pp. 17–23. American Society of Civil Engineers.

Sanchez-Salinero, I., Roesset, J. M., Shao, K. Y., Stokoe, K.H II & Rix, G. J. (1987). Analytical evaluation of variables affecting surface wave testing of pavements. *Transp. Res. Rec.*, No. 1136, 86–95.

Sheriff, R. E. (1991). *Encyclopedic dictionary of exploration geophysics*, 3rd edn. Tulsa, OK: Society of Exploration Geophysicists.

Sheriff, R. E. & Geldart, L. P. (1983). *Exploration seismology*, vols 1 and 2. New York: Cambridge University Press.

Sheu, J. C., Stokoe, K. H. II & Roesset, J.M. (1988). Effect of reflected waves in SASW testing of pavements. *Transp. Res. Rec.*, No. 1196, 51–61.

Song, Y. Y., Castagna, J. P., Black, R. A. & Knapp, R. W. (1989). Sensitivity of near-surface shear-wave velocity determination from Rayleigh and Love waves. *Expanded Abstracts of 59th Ann. Mtng of Society of Exploration Geophysicists, Dallas*, 509–512.

Stokoe, K. H. II & Nazarian, S. (1983). Effectiveness of ground improvement from spectral analysis of surface waves. *Proc. 8th Eur. Conf. Soil Mech. Found. Engng, Helsinki* **1**, 91–95.

Stokoe K. H II, Rix, G. J & Nazarian, S. (1989). In situ seismic testing with surface wave. *Proc. 12th Int. Conf. Soil Mech. Found. Engng, Rio de Janeiro*, 331–334.

Stokoe K. H. II, Wright, G. W., Bay, J. A. & Roesset, J. M. (1994). Characterization of geotechnical sites by SASW method. In *Geophysical characterization of sites* (ed. R. D. Woods), ISSMFE Technical Committee 10, pp. 15–25. New Delhi: Oxford Publishers.

Tokimatsu, K., Kuwayama, S., Tamura, S. & Miyadera, Y. (1991). V_S determination from steady state Rayleigh wave method. *Soils Found.* **31**, No. 2, 153–163.

Turner, M. A. (1990). *Near-surface velocity reconstruction using surface wave inversion*. MS thesis, Department of Geology and Geophysics, University of Utah.

Xia, J., Miller, R. D. & Park, C. B. (1997). Estimation of shear wave velocity in a compressible Gibson half-space by inverting Rayleigh wave phase velocity. *Expanded Abstracts of 67th Ann. Mtng of Society of Exploration Geophysicists, Dallas*, 1917–1920.

Xia, J., Miller, R. D. & Park, C. B. (1998). Construction of vertical seismic section of near-surface shear-wave velocity from ground roll. *Expanded Abstracts Society of Exploration Geophysicists/ AEGE/CPS, Beijing*, 29–33.

Xia, J., Miller, R. D. & Park, C. B. (1999). Estimation of near-surface shear-wave velocity by inversion of Rayleigh waves. *Geophysics* **64**, No. 3, 691–700.

Xia, J., Miller, R. D., Park, C. B., Hunter, J. A. & Harris, J. B. (2000a). Comparing shear-wave velocity profiles from MASW with borehole measurements in unconsolidated sediments, Fraser River Delta, BC, Canada. *J. Environ. Engng Geophys.* **5**, No. 3, 1–13.

Xia, J., Miller, R. D., Park, C. B. & Ivanov, J. (2000b). Construction of 2-D vertical shear-wave velocity field by the multichannel analysis of surface wave technique: *Proceedings of the symposium on the application of geophysics to engineering and environmental problems (SAGEEP 2000)*, Arlington, VA, pp. 1197–1206.

Xia, J., Miller, R. D., Park, C. B., Hunter, J. A., Harris, J. B. & Ivanov, J. (2002a). Comparing shear-wave velocity profiles from multichannel analysis of surface wave with borehole measurements. *Soil Dynam. Earthquake Engng* **22**, No. 3, 181–190.

Xia, J., Miller, R. D., Park, C. B., Wightman, E. & Nigbor, R. (2002b). A pitfall in shallow shear-wave refraction surveying. *J. Appl. Geophys.* **51**, No. 1, 1–9.

Xia, J., Miller, R. D., Park, C. B. & Gang, T. (2003). Inversion of high frequency surface waves with fundamental and higher modes. *J. Appl. Geophys.* **52**, No. 1–2, 11–23.